HYPERSONIC VEHICLE CONSTRUCTION & ANALYSIS USING 2D FLOW FIELDS

Haile Lindsay and Frederick Ferguson, Stephen Akwaboa
North Carolina A&T State University, Greensboro, North Carolina, 27411

and

Hydar Apdin
Michelin North America, Greenville, South Carolina, 29615

ABSTRACT

With the push in manned hypersonic flight and hypersonic vehicle design, it has been brought to the forefront that vehicles are needed that can be utilized as air-breathing single stage to orbit (SSTO) next generation vehicles that can sustain flights in the range of Mach 4 – 20. This paper describes the development of these hypersonic vehicles, utilizing a FORTRAN solver that would use a Darwinian approach, meaning that the design of the vehicles would be a product of its own environment (two – dimensional shockwaves and freestream conditions), that would utilize a minimum set of requirements or inputs prescribed by the user to construct a class of hypersonic vehicles that would yield the optimal aerodynamic parameters that include lift, drag, lift over drag ratio, calculate the forces acting upon the vehicle, find the areas and volume of the vehicle, and be able to access space at will and for a wide set of missions utilizing fundamental aerodynamic and thermodynamic principles that include oblique shockwave relations (in the design of the forebody), 1-D flow with friction and heat addition (in the design of the combustor), and Prandtl – Meyer Expansion Wave Theory (in the design of the nozzle). In designing these vehicles, equations of lines along specially developed subroutines were utilized and the waverider of interest is the inlet waverider. In addition, the design concept that is being utilized in this study has the potential to generate configurations of interest to the hypersonic community.

NOMENCLATURE

α_2 = coefficient that controls the location of the second shockwave
α_4 = coefficient that controls the length of the nozzle
β = shock wave angle
C_f = skin friction coefficient
D = Drag, force component parallel to the freestream velocity
γ = specific heats ratio
h = flight altitude
II = number of points utilized to get the maximum number of useful streamlines
j_w = number of points used to create the wedge portion of the inlet waverider
j_{start} = value of the starting point to create the wings on the inlet waverider
L = Lift, force component perpendicular to the freestream velocity

M = Mach number
Φ = caret angle
θ = wedge angle
p = pressure
S = Surface area
τ = shear stress
T = temperature
u = velocity component parallel to the freestream velocity
v = velocity component perpendicular to the freestream velocity
V = Volume
$\acute{\omega}$ = viscosity exponent
WL = waverider length

I. INTRODUCTION

Aviation has been in existence for over a hundred years since the Wright Brothers flew at Kitty Hawk, North Carolina and when it comes down to airplanes, space shuttles, rockets, etc., the trend in aviation design is to achieve greater speed. The earliest frontier of speed dealt with supersonic aircrafts traveling at Mach 2 – 3 (or two to three times the speed of sound). At this particular day and age, the push is to create aircrafts that will travel from Mach 5 – 25 or at hypersonic speed. One of the important uses of developing vehicles that fly at hypersonic speed is for faster intercontinental travel. For example, being able to potentially fly from New York to Tokyo in less than an hour as the X-30 was projected to do. Another important use of developing hypersonic vehicles is to be able to fly and enter into space without any problems. In addition to the other uses of hypersonic vehicles that include business jets, military use, and high speed cargo planes, President George W. Bush in 2004, has declared a new initiative on deep space exploration and that goal is to ultimately retire the space shuttle by the year 2010 and an example of this hypersonic vehicle can be seen in Figure 1. The key to this initiative becoming successful requires that the vehicle be accessible to travel to space, be economical enough to travel, reusable, and capable of transporting 25,000 lbs. of cargo to and from the International Space Station, Ref 1. It is also critical that these hypersonic vehicles demonstrate the use of the airframe-integrated ramjet/scramjet engine technology followed by the development of hypersonic aerodynamics and validation of design tools for air – breathing hypersonic vehicles, Ref 2. Within the last forty to fifty years, a set of vehicles have been produced in order to achieve the goal of hypersonic vehicles as reality and these vehicles are known as waveriders. A waverider is any hypersonic vehicle that uses it own shockwave (inverse design approach) to improve its overall aerodynamic performance, Ref 3. These vehicles are practical at higher Mach numbers because the shockwave must remain close to the surface, a quality of hypersonic flow. Various types of waveriders include the caret and conical flow.

Figure 1: Hypersonic Missile Configuration

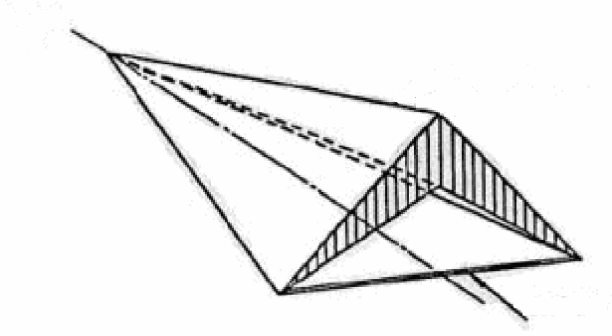

Figure 2: Caret Waverider

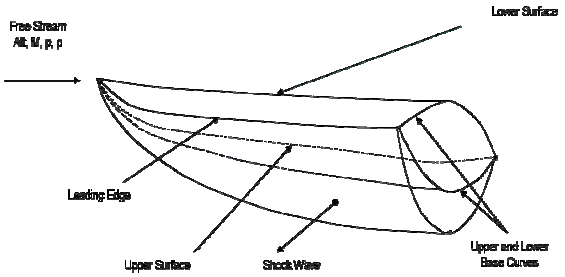

Figure 3: Conical Flow Waverider

In designing hypersonic vehicles, to test the aerodynamic performance of the vehicles, it's important to use the Kuchemann curves (see Figure 4) and it is a set of plots where on the x axis is Mach number and on the y axis is the maximum value of lift over drag. As one would look at this graph below, it is noticeable to see that the white dots trimmed in black fall under the solid line Kuchemann curve and that's due to strong viscous effects (which leads to high skin friction drag) and strong shockwaves (which leads to high wave drag) that they suffer when flying at those high speeds. The goal of using these curves is to create a vehicle that demonstrates an aerodynamic performance within the two curves; both the solid and dotted curves or exceed what's being shown. In theory, the dashed curve cannot be exceeded unless there's no engine in the vehicle, Ref 4. The goal of this paper is to describe the waverider design concept to that of constructing a complete hypersonic vehicle, which comprise of the fore-body, nozzle, scramjet propulsion system and wings.

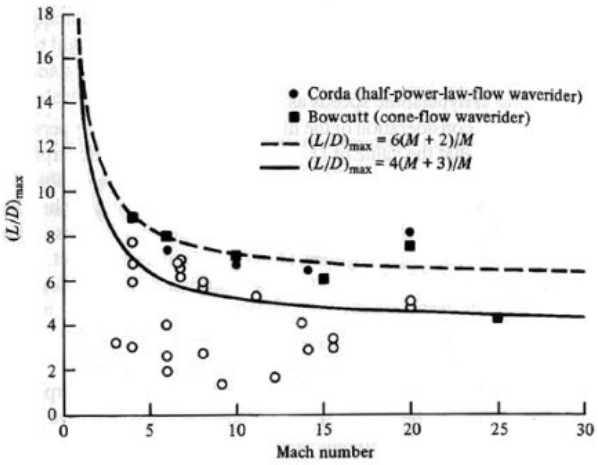

Figure 4: Kuchemann Curve

II. Design Approach

The basic approach to the effective design of waverider configurations comes mainly from the exact solution of the oblique shock-wave theory. To understand this concept, refer to Figure 5. Consider a shockwave in a supersonic flow that is induced by the wedge, *ABC*. As indicated in Figure 1, in the case of an inverse design approach, for a given Mach number, *M*, and for a given oblique shock wave angle, β, there is a corresponding wedge deflection angle, θ, which decides the basic geometry of the wedge. In addition, for any point, *A*, on the shockwave, for the purposes of this analysis, two lines emanate down stream, namely, line *AB*, a free stream streamline from which the upper vehicle surface will be carved and line *AC*, from which the lower vehicle surface is carved. A typical waverider is derived from these two surfaces. Using this approach, each point lying on a leading edge curve that lies on the shock wave can contribute to the construction of the resulting waverider geometry. This concept is illustrated in

Figure 2 in the case of a wedge. This design concept is not limited to the wedge configuration. In fact, an entire vehicle can be generated using this technique.

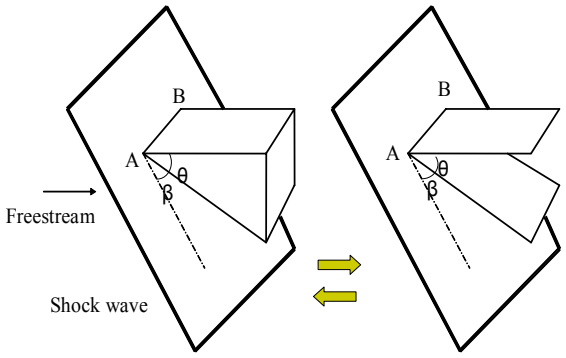

Figure 5: Waverider 2D Design

II.A. BASIC PLANE GENERATION

In general, a waverider configuration derived from 2-D shocks is composed of intersecting planes and surfaces. Within this paper, the surfaces were created using the simple equation of a line stated in the following manner:

$$y = mx + b \tag{1}$$

where m is the slope and it has varying values that may include the tangent of the shock angle or the tangent of the wedge angle, etc. and b is the intercept of the line along the y - axis. Based on the geometric principles underlined in this equation, a group of subroutines were developed in FORTRAN. These routines are programmed to handle the waverider design process, by generating basic planes and lines as required.

II.B. HYPERSONIC FOREBODY GENERATION

A typical caret shaped waverider, illustrated in Figure 2, is generated using the principles described earlier. In this case of a caret shaped waverider the shock wave is prescribed along with the leading edge lines, namely, *EF* and *EG*. Next, the equation for the line *EH* is prescribed using the free stream information. The point, *HL*, can be calculated through the use of the shock wave relations. Once these basic line equations are obtained the appropriate surfaces, *EHG*, *EHLG*, *EFF* and *EEFHL* are constructed through the appropriate use of the subroutine *caret*. It is of interest to note that the resulting caret waverider is constructed such that it induces the prescribed shock wave. This concept was demonstrated in Ref. 5-8.

This section discusses an innovative approach to the generation of a waverider derived forebody that can be used to prepare the hypersonic flow for scramjet processing. For instance, Figure 4 illustrates the shape of a hypersonic forebody that was constructed using

this design philosophy. Splitting the caret waverider, which is illustrated in Figure 2, at line EH and adding an appropriate wedge in between can lead to the construct of this idealized forebody configuration seen in Figure 6.

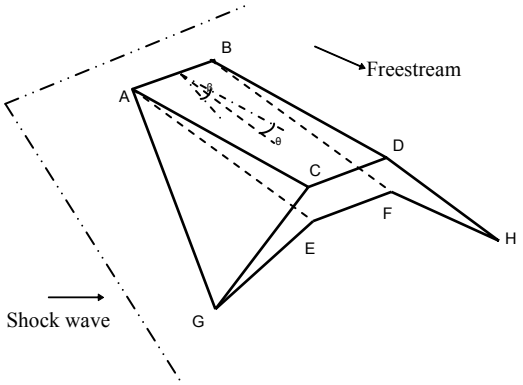

Figure 6: A Hypersonic Forebody

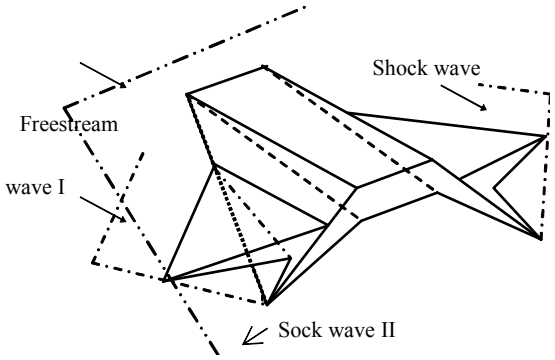

Figure 7: An Inlet Waverider

Star-shaped waveriders are constructed from the basic caret shape, shown in Figure 2. One caret waverider attached to another in an appropriate manner can form a star-shaped waverider. In this case, two separate shockwaves are required. The multiple uses of shockwaves as required by of the star-shaped waveriders provide great flexibility and versatility that are very important to aircraft designers. In fact, this capability is exploited in Ref. 8, to expand the waverider design space and to conduct scramjet-forebody integration studies. A hypersonic vehicle configuration with waverider derived wings is shown in Figure 7. It is composed of an inlet as main body and two star-shaped geometries as wings and this work was done in subroutine *inlet*. A total of three shockwaves are attached to this vehicle. Besides the added lift, the wings provide more volume to the entire vehicle.

II. C. DESIGN OF THE SCRAMJET COMBUSTOR

The combustor design can follow the concept of a constant area or the concept of a variable area duct. The inlet plane to the scramjet combustor equals the outlet plane of the forebody, but the exit area can be designer created. The length of the duct is based on the design conditions appropriate for the user's predetermined scramjet model and the combustor generated by this design methodology is displayed in Figure 8.

At the conclusion of the forebody design phase, not only is the shape of the inlet to the scramjet combustor known, but also the mass flow rate and for efficient combustor designs, it is required that the mass flow ejected from the scramjet does so under choked conditions. In satisfying these conditions, certain assumptions are made. First of all, effective mixing is assumed so that completed combustion occurs within the combustor and just prior to the scramjet exit plane. This methodology can be described through the following empirical equation that is found in Ref. 9:

$$\tau_R = 0.145\, p^{-0.0035} e^{0.0001 T_0} \tag{2}$$

where τ_R represents the inverse of the reaction time, p represents the average pressure, and T_0 is the total temperature within the scramjet. It is also noted that the combustion time will

determine the length of the combustor, since the combustor length is expressed as the following:

$$L_{scramjet} = \frac{V_{avg}}{1/t} = \left(\frac{M_{in} + M_{out}}{2} \right) \frac{\sqrt{\gamma R_{gas} T_{in}}}{\tau_R} \tag{3}$$

where γ and R_{gas} are the ratio of specific heats and the universal gas constant, M_{in}, M_{out}, and T_{in} represents the average Mach numbers and temperature entering and leaving the scramjet. Once equations (2) and (3) are rearranged and a few constants are manipulated, the following equation is acquired:

$$\left(\frac{L}{H} \right)_{scramjet} = \frac{C(M_{ref} + 1)\sqrt{\gamma R_{gas} T_{ref}}}{p^{-0.0035} e^{0.0001 T_0}} \tag{4}$$

In equation 4, the quantities with the subscript 'ref' such as M_{ref}, T_{ref}, P_{ref}, and $T_{0,ref}$ represent the average thermodynamic parameters at the entrance of the combustor, while the symbol C is representative of a constant value and the length of the scramjet is very dependent upon the nature of the thermodynamic processes within the combustor.

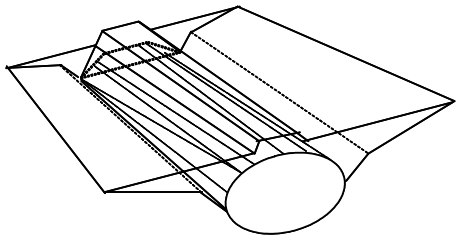

Figure 8: Typical Scramjet Combustor

II.D. NOZZLE DESIGN

The method of characteristics (MOC) is used to define the scramjet nozzle. Here again, the inlet plane to the nozzle is the same as the combustor's exit plane. However at this plane the conditions of choked quasi-1D flow is assumed. In addition, this design analysis requires that the exit plane of the nozzle has a Mach number equals to that of the freestream. With these design conditions it can easily be shown that the nozzle shape, $y = y(x)$, can be constructed in accordance with the following equation:

$$\frac{dy}{dx} = \tan\left(\theta \pm \mu \right) \tag{5}$$

where the θ and μ, are functions of the local Mach number within the nozzle. Further, in this analysis based on the MOC, θ and μ can be defined as follows:

$$\theta = \tan^{-1}(v/u) \tag{6}$$

$$\mu = \sin^{-1}(1/M) \tag{7}$$

and where *u* and *v* are velocity components in *X* and *Y* direction, respectively. It should be noted that in the analysis of the nozzle contour, scaling factors in the x and y directions were used. This is because the nozzle contour produced by the method of characteristics (MOC) was a bit out of proportion in comparison to the other components of the scramjet. Based on the freestream conditions and the location of the second ramp the overall height of the scramjet ($H_{overall}$) was found. The MOC produced a nozzle contour whose overall height and length were $L_{nozzle,MOC}$ and $H_{nozzle,MOC}$. The scaling factors in the x direction (SF_x) and in the y directions (SF_y) are thus defined respectively as:

$$SF_x = \frac{L_{assumed}}{L_{nozzle,MOC}} \tag{8}$$

and

$$SF_y = \frac{H_{overall}}{H_{nozzle,MOC}} \tag{9}$$

where $L_{assumed}$ was the assumed length of the nozzle. Shown below in Figure 9 and 10, are the plots of scaled and unscaled nozzle at Mach 16 with a shock angle of 16 degrees.

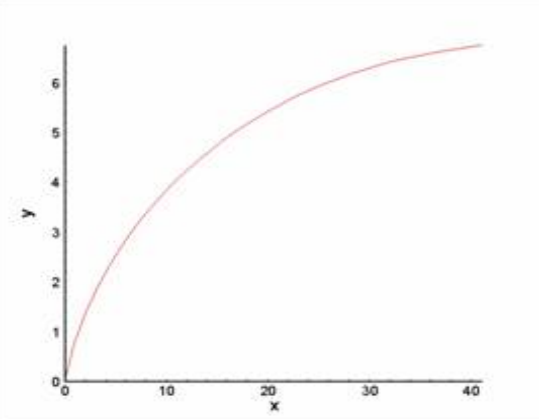

Figure 9: Unscaled Plot of the Nozzle Contour

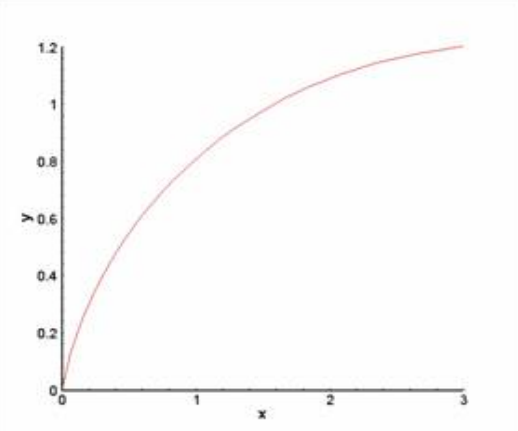

Figure 10: Scaled Plot of the Nozzle Contour

III. AERODYNAMIC FORCES EVALUATION

The aerodynamic analysis of the generated hypersonic vehicle was conducted through the use of two separate but complementary analyses procedures. Viscous and inviscid analyses were conducted separately, since the total corresponding force acting on the vehicle can be expressed as follows,

$$\overline{F} = \overline{F}(\mathrm{P}, \tau) \tag{10}$$

where P is the pressure and τ is the shear stress. In fact, the aerodynamic force is obtained through the integration of the local pressure and shear stress over the vehicle's surface through the use of the expression,

$$\overline{F} = \iint_S \mathrm{f}(\mathrm{P}, \tau)\, d\overline{S} \qquad (11)$$

where dS defines an infinitesimal surface element. The force x-components contribute to the vehicle's total drag and the y-components contribute to vehicle's total lift. However, the force component in z-direction is neglected in this study due to the fact that the forces acting in opposite direction have the same magnitude.

The lift and drag forces acting on the hypersonic vehicle configuration can be estimated by analyzing the forces due to pressure and shear stress as illustrated in Figure 11. In fact, the expression used to calculate the lift and drag forces in this particular study are as follows:

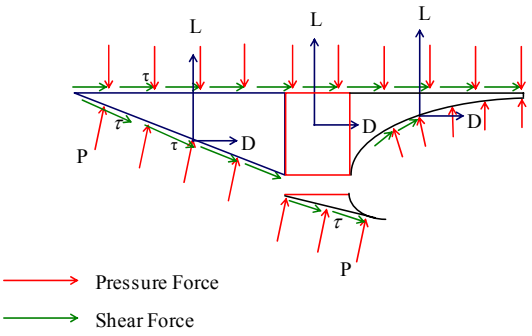

Figure 11: Aerothermodynamic Analysis

$$L = P_{avg} \,.\, Area_{plan} + \tau_{avg} \,.\, Area_{base} \qquad (12)$$

$$D = P_{avg} \,.\, Area_{base} + \tau_{avg} \,.\, Area_{plan} \qquad (13)$$

where P_{avg} and τ_{avg} represent the average aerodynamic and viscous forces due to the pressure and shear stress acting on the base and plan form projected surfaces of the aircraft, respectively. Finally, the lift and drag coefficients are evaluated by using the following expressions,

$$C_L = \frac{L}{q_\infty S} \qquad (14)$$

$$C_D = \frac{D}{q_\infty S} \qquad (15)$$

where q_∞ is the freestream dynamic pressure.

III.A. AVERAGE PRESSURE ESTIMATION

An estimation of the local pressure distribution, $P = P_{i,j}; (1 \le i \le II, 1 \le j \le JJ)$, on the hypersonic vehicle is conducted through the use of the value of the pressure after the linear shockwave (constant at all points behind the shock) using the oblique shockwave relations and it is expressed in the following manner:

$$P_2 = P_1\left(1 + \frac{2\gamma}{\gamma+1}\left(M_{n,1}{}^2 - 1\right)\right) \qquad (16)$$

where the P_1 is just the freestream pressure and P_2 is the pressure behind the shock. Finally, the average pressure is determined as follows:

$$P_{avg} = \frac{\sum_{i,j} P_{i,j}}{number\ of\ grid\ points} \tag{17}$$

III.B. AVERAGE SHEAR STRESS ESTIMATION

The expressions for the local skin friction coefficient, c_f for the laminar and turbulent flows are given by Ref. 4 in the form:

$$C_{f,st,lam} = \frac{0.664}{\sqrt{\mathrm{Re}_{st}}}\left[0.45 + 0.55\frac{T_w}{T_\infty} + 0.09(\gamma-1)\sqrt{\mathrm{Pr}_\infty} M_{st}^{\ 2}\right]^{-0.25} \tag{18}$$

$$C_{f,st,turb} = \frac{0.0592}{\mathrm{Re}_{st}^{\ 1/5}}\left[1 + \frac{(\gamma-1)}{2}\mathrm{Pr}_\infty^{\ 0.3333} M_{st}^{\ 2}\right]^{0.55} * \left(\frac{T_w}{T_\infty}\right)^{-0.21} \tag{19}$$

where Re_x is the local Reynolds number and ω is the exponent for the viscosity variation. Using the expressions in (18) and (19) the appropriate local shear stress, τ_w, $\tau_w = \tau_{i,j}; (1 \le i \le II, 1 \le j \le JJ)$ quantity; laminar or turbulent, can be evaluated as follows:

$$\tau_w = c_f q_e \tag{20}$$

In the present waverider analysis, the values for $\gamma, \omega,$ and Pr are chosen as follows[7-8, 11-14]:

$$\begin{aligned} &\gamma = 1.4 \\ &\omega = 0.75 \\ &\mathrm{Pr} = \begin{cases} 0.71 & \text{laminar flow} \\ 0.89 & \text{turbulent flow} \end{cases} \end{aligned} \tag{21}$$

The boundary layer transition the relationship given by[7-8, 11-14]:

$$\log_{10} \mathrm{Re}_{z,tr} = 6.421\, e^{(1.209 * 10^{-4} M_e^{\ 2.641})} \tag{22}$$

Finally, the average shear stress on the vehicle surface is evaluated using the following equations using an elemental area (see Figure 12 below):

$$f_{avg}^{element} = \frac{(\tau_a + \tau_b + \tau_c)}{3} * A \tag{23}$$

$$\tau_{avg} = \frac{\sum_{i,j} f_{avg}^{element}}{Total\ wetted\ area} \tag{24}$$

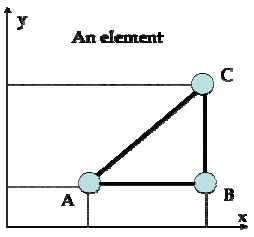

Figure 12: Elemental Triangle

where τ_a, τ_b, and τ_c is the shear stresses at points A, B, and C in the elemental triangle, $f_{avg}^{element}$ is the elemental force and τ_{avg} is the average shear stress.

III.C. PROJECTED AND WETTED AREAS

The waverider shapes are often not shapes of which the area can be easily taken. Therefore the Triangulation Method is used. With the Triangulation Method, the surface of the waverider is divided into many triangle-shaped elements (as shown in Figure 12). The sides of the element are calculated as follows:

$$\begin{aligned} AB &= \left\{\lambda_x\left(X_A - X_B\right)^2 + \lambda_y\left(Y_A - Y_B\right)^2 + \lambda_z\left(Z_A - Z_B\right)^2\right\}^{0.5} \\ AC &= \left\{\lambda_x\left(X_A - X_C\right)^2 + \lambda_y\left(Y_A - Y_C\right)^2 + \lambda_z\left(Z_A - Z_C\right)^2\right\}^{0.5} \\ BC &= \left\{\lambda_x\left(X_B - X_C\right)^2 + \lambda_y\left(Y_B - Y_C\right)^2 + \lambda_z\left(Z_B - Z_C\right)^2\right\}^{0.5} \end{aligned} \tag{25}$$

where λ_m equals 1 or 0 if the projection is in the m direction. The projected area is calculated with these expressions:

$$\begin{aligned} t &= (AB + BC + AC)/2 \\ A_{element} &= \left(t*(t-AB)*(t-BC)*(t-AC)\right)^{0.5} \\ S_m &= \sum\sum A_{element} \end{aligned} \tag{26}$$

For the average shear stress calculations, the wetted areas can also be calculated with equations 25 and 26, keeping $\lambda = 1$.

IV. HYPERSONIC VEHICLE FLOW PATH ANALYSIS

While the concept behind the scramjet is very simple, the practical ramifications of hypersonic travel are quite formidable. A couple of the challenges are supersonic fuel-air mixing, and heat dissipation both from the air friction and the internal combustion. Consequently, the flow path of the incoming air needs to be extremely precise to minimize hot spots. By far the biggest challenges the scramjet face are those arising from the intense operational temperatures. Since the air entering the engine is already heated by friction with the engine walls, combustion chamber temperatures would exceed 5000 degrees Fahrenheit, if left unchecked. At these temperatures most metals melt, and air and fuel become ionized so that the physics of their behavior becomes unpredictable. Even when the heat is dissipated efficiently, the structural strength of most metals declines dramatically at the operating temperatures, so a different type of heat conducting material has to be used. Composites are the material of choice, but only after extended research and testing can a suitable material be developed. In practice, aircraft weight has to be kept to a minimum, while maintaining structural strength and rigidity to dampen the tremendous vibrations that can occur at

hypersonic speeds. Due to these and other inherent design complexities, progress in the field of scramjet research has been extremely slow. However, due to recent findings of Russian and French scramjet experiments, the successful experimental scramjet flights conducted by the Australian and Americans, these are renewed interest in this area of propulsion.

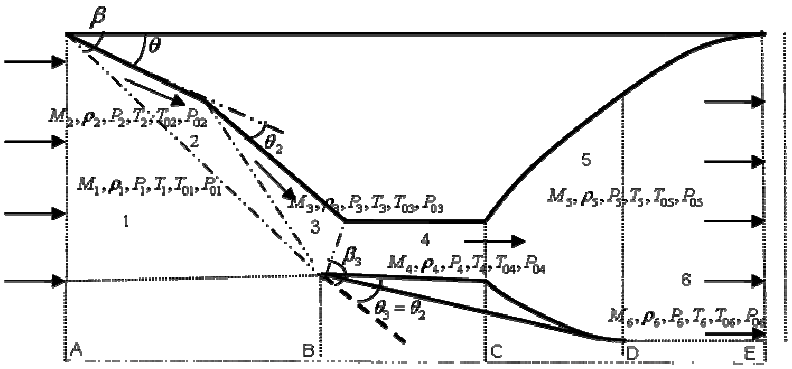

Figure 13: Hypersonic Vehicle Flow Path Analysis

IV.A. OBLIQUE SHOCK WAVE CALCULATIONS

This section briefly describes the basic equations needed for the hypersonic vehicle flow path analysis illustrated through the use of a control volume in Figure 13. The hypersonic vehicle flow path analysis involves the evaluation of the flow field properties in the six different regions that makes up the flow path control volume. Further, each separated with the virtual surfaces, AA', BB', CC', DD' and EE'. Evaluation of the flow fields in regions 1 through 4 are relatively straight forward and can be easily accomplished through the use of equations (27) through (33) listed in Table 1. The other oblique shock relations[9] of interest to this study are listed below:

Table 1. Equations Used in Aerodynamic Analysis

$$M_{n,1} = M_1 \sin\beta \quad (27)$$

$$M_{n,2}^2 = \frac{1+[(\gamma-1)/2]M_{n,1}^2}{\gamma M_{n,1}^2 - (\gamma-1)/2} \quad (28)$$

$$M_2 = \frac{M_{n,2}}{\sin(\beta-\theta)} \quad (29)$$

$$\frac{\rho_2}{\rho_1} = \frac{(\gamma+1)M_{n,1}^2}{2+(\gamma-1)M_{n,1}^2} \quad (30)$$

$$\frac{p_2}{p_1} = 1 + \frac{2\gamma}{\gamma+1}(M_{n,1}^2 - 1) \quad (31)$$

$$\frac{T_2}{T_1} = \frac{p_2}{p_1}\frac{\rho_1}{\rho_2} \quad (32)$$

$$\frac{P_0}{P} = (1+\frac{\gamma-1}{2}M^2)^{\gamma/(\gamma-1)} \quad (33)$$

Appropriate care must be taken during the evaluation of equations (25) through (31) as it is applied to each zone boundary; namely, *1-2, 2-3* and *3-4*. In addition, precautions must be taken as the following $\theta-\beta-Mach$ relations;

$$\tan\theta = 2\cot\beta \frac{M_1^2 \sin^2\beta - 1}{M_1^2(\gamma + \cos 2\beta) + 2} \tag{32}$$

are applied.

IV.B. ANALYSIS AND PERFORMANCE OF THE SCRAMJET

In conducting this analysis, it is safe to assume that the flow field properties at the entrance of the scramjet are known and from here, the goal is to evaluate the average flow field properties in the scramjet upon the basis of an ideal representation of the combustion process.

The stoichiometric fuel to air ratio, f_{st}, is the ideal upper limit for the fuel to air ratio that corresponds to complete mutual combustion of all the oxygen that is presented in the air with all the reactants available in the fuel. The fundamental assumption is that anything less would not take full advantage of the available oxygen, and anything less would waste the fuel that could not be burned. Since almost all the fuels under consideration for hypersonic flights are hydrocarbons, the general chemical equation for their complete combustion with the air available in Earth's atmosphere is given by

$$C_x H_y + \left(x + \frac{y}{4}\right)\left(O_2 + \frac{79}{21}N_2\right) \rightarrow xCO_2 + \frac{y}{2}H_2O + \frac{79}{21}\left(x + \frac{y}{4}\right)N_2 \tag{34}$$

Using this expression, the stoichiometric fuel to air ratio, f_{st} can be obtained in the form

$$f_{st} = \frac{36x + 3y}{103(4x + y)} \tag{35}$$

In this analysis, hydrogen is the scramjet fuel of choice, and it is assumed that the stoichiometric fuel to air ratio is equal to the fuel to air ratio, ($f_{st} = f$); as such, x and y take on the values of 0 and 2, yielding a value of $f_{st} = 0.0291$.

The rate at which chemical reactions create energy, $\dot{q}_{\max}$ available to the engine cycle is described as, $\dot{q}_{\max} = f_{st}\dot{m}_{inlet}h_{PR}$, where $h_{PR} = 119{,}954\ kJ/Kg$ when hydrogen is used to fuel the scramjet. The quantity, $\dot{q}_{\max}$, obtained from this simplified analysis will be used in the evaluation of the energy equation later in this paper.

In determining the length of the scramjet, three major principles are utilized: 1-D mass flow, 1-D flow with heat addition and 1-D momentum equation for choked flow with friction. The 1-D mass flow equation is written in the following form:

$$\dot{m}_{ref} = A_{ref}\ p_{ref}\ M_{ref}\sqrt{\frac{\gamma}{RT_{ref}}} \tag{36}$$

where A represents the area of the scramjet duct $\dot{m}_{ref}$ represents the mass flow rate entering the scramjet, $\dot{m}_{inlet}$. Based from findings in Ref. 6, the expression to calculate the maximum heat flux is given in this notation:

$$\dot{q}_{\max} = C_p \, T_{ref} \frac{\left(M^2_{ref} - 1 \right)^2}{2 M^2_{ref} \left(1 + \gamma \right)} \tag{37}$$

where C_p is the specific heat that is calculated using the following equation:

$$C_p = \frac{\gamma * R_{gas}}{\gamma - 1} \tag{38}$$

Once the maximum heat flux is known, a careful review of the conservation equations shows that the following 'ref' set of flow parameters, P_{ref}, T_{ref}, and $T_{0,\,ref}$ can be calculated from the following equations:

$$T_{ref} = \frac{2 \dot{q}_{\max} (\gamma + 1) M^2_{ref}}{\dot{m}_{inlet} C_p \left(M^2_{ref} - 1 \right)^2} \tag{39}$$

$$T_{0,ref} = T_{ref} \left(1 + \frac{\gamma - 1}{2} M^2_{ref} \right) \tag{40}$$

$$P_{ref} = \frac{\dot{m}_{inlet} \sqrt{\gamma R_{gas} T_{ref}}}{\gamma A M_{ref}} \tag{41}$$

where the only unknown is M_{ref}. This value can be determined by using the last of the three major principles mentioned earlier which is 1-D momentum equation for choked flow with friction and it is given in the form,

$$L_{scramjet} = \frac{h_{inlet}}{4 f} \left\{ \frac{1 - M^2_{ref}}{\gamma M^2_{ref}} + \frac{\gamma + 1}{2\gamma} \ln \left(\frac{(\gamma + 1) M^2_{ref}}{2 + (\gamma - 1) M^2_{ref}} \right) \right\} \tag{42}$$

In this paper, the goal is to create a scramjet that is half the length of the forebody and Figure 14 demonstrates the action of both 1-D flow with friction and 1-D flow with heat addition at Mach 6, ß = 40°, and the forebody length is equal to 1.

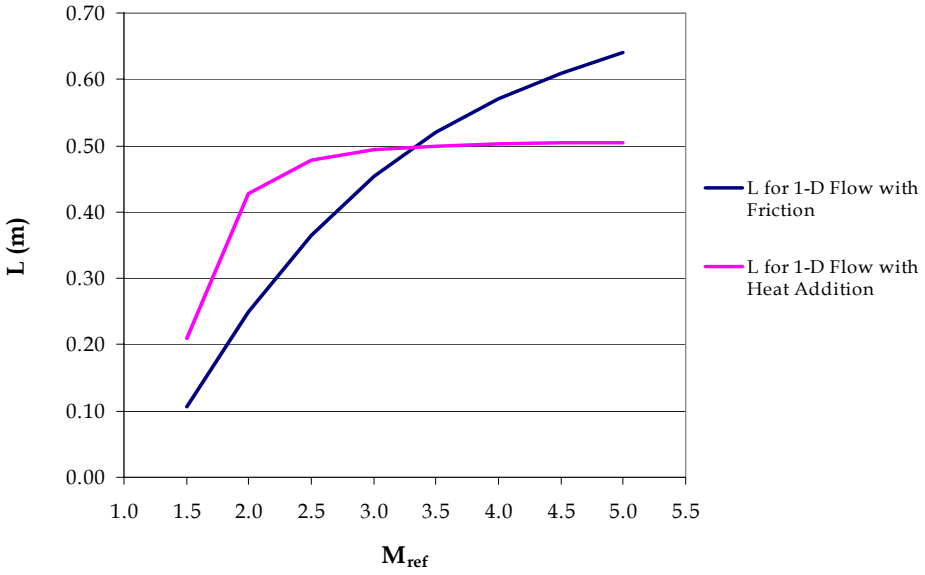

Figure 14: M_{ref} vs. Scramjet Length for 1-D Flow with Friction and Flow with Heat Addition

V. RESULTS AND ANALYSIS

In this section the code is used to identify the design variables and their sensitivity with respects to the vehicle's aerodynamic performance. Lift over drag (L/D) analysis was conducted with respect to two sets of design variables; namely, the vehicle geometric properties, and the freestream Mach number. The geometric variable considered as part of this analysis is the forebody or wedge deflection angle, θ. The effects of the Mach number and the wedge deflection angle on the vehicle geometric properties, such as volume and wetted surface area, were also studied. In this paper, the values that are forthcoming only represent the values at the forebody.

Table 2. Example of the Inputs and Outputs of the Program

Inputs		Outputs	
Mach Number	6.0	Wedge Angle(Θ)	8.3°
Altitude (H)	30 km	Lift	1502 N
Shock Angle (ß)	16°	Lift Coefficient (C_l)	0.088
Forebody Length (WL)	1 m	Drag	321 N
Inlet Width(W_i)	0.2	Drag Coefficient (C_d)	0.019
2nd Shockwave Factor (α_2)	0.5	L/D	4.68
Nozzle Length Factor (α_4)	0.6	Volume (m^3)	5.2 x 10^{-2}

V.A: PERFORMANCE ANALYSIS OF THE HYPERSONIC VEHICLE

A typical input set used by this code, and a typical output data set generated by it are listed in Table 2. In addition, a typical hypersonic vehicle generated from the use of this data is shown in Figure 15. Figure 16 displays a plot of shock angle ß vs. L/D ranging from 16 degrees to 24 degrees and the trend to see here is that as the shock angle increases, the lift over drag ratio decreases and therefore it allows one to understand that the vehicle's height would be slender.

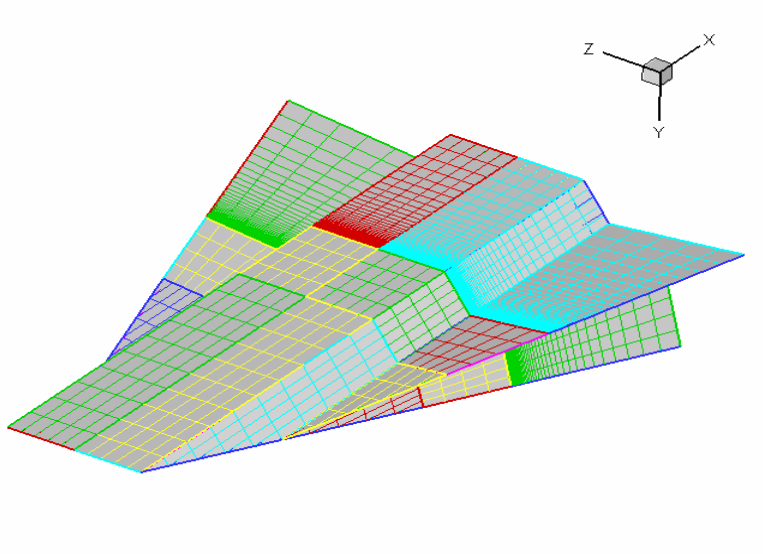

Figure 15: Completed Hypersonic Vehicle

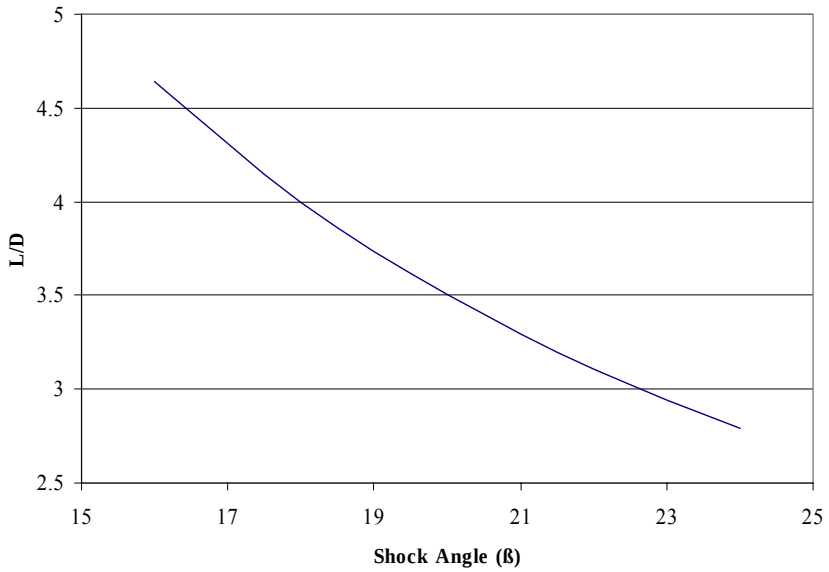

Figure 16: L/D Ratio vs. Shock Angle

V.B: L/D ANALYSIS OF THE HYPERSONIC VEHICLE

Using the analytical capabilities of the code developed herein, a preliminary design analysis was conducted and the performance outcome can also be represented as design points on the Kuchemann curves illustrated in Figure 17.

The L/D hypersonic barrier based on actual flight test data given in Ref. 17 is represented by the following relationship:

$$\left(\frac{L}{D}\right)_{\max} = \frac{4(M+3)}{M} \tag{43}$$

Equation (43) is depicted in Figure 17 by a blue line. However, a much closer representation of the L/D ratio for viscous optimized waverider is given in Ref. 7; the curve is also shown in Figure 21 by the blue-gray line, which represents the correlation:

$$\left(\frac{L}{D}\right)_{\max} = \frac{6(M+2)}{M} \tag{44}$$

The L/D ratio for the hypersonic vehicles generated during this study using the arbitrary input data sets tabulated in Table 2 is depicted through the blue line in Figure 17. It is of interest to note that for the vehicles constructed herein, delivers L/D performance ratios within the values predicted by equations (43) and (44), and it has a trend similar to the Kuchemann curves.

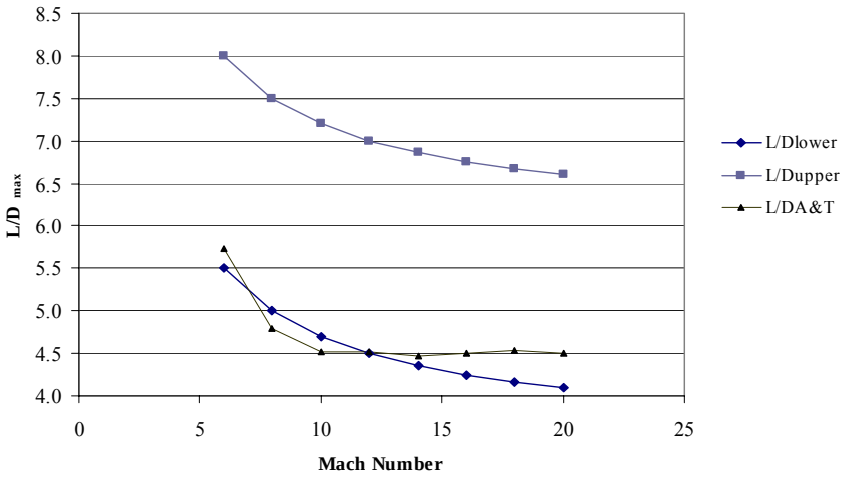

Figure 17: L/D ratio vs. Mach number

VI. CONCLUSION

The design process for constructing waverider derived hypersonic vehicle is outlined, and documented in the creation of a FORTRAN based program. The methods used to evaluate the lift and drag characteristics of the vehicle are discussed, and their relationship to the local pressure and shear stress distributions over the vehicle surface are documented. Further, the algorithms used for the calculations of the vehicle aerodynamic performance are described in detail in this paper. In addition, the basic equations used for the evaluations of the geometric characteristic of the vehicle are also documented.

Using the newly developed solver, the volume and the surface area of the hypersonic configuration, in addition to its lift and drag coefficients, and its L/D ratio, were analyzed with respects to certain design parameters. Further, the L/D ratio was studied as it relates to changes in the geometric variables. The L/D versus the Mach number behavior was compared with the Kuchemann barriers and the work done in this research holds its own through only the use of the forebody and in the future the goal is to complete the analysis with the other two major components.

Finally, the hypersonic vehicle code was used to identify the design variables; including both aerodynamic and geometric parameters, that are most sensitivity to the overall performance of the resulting vehicle.

VII. REFERENCES

[1] Apdin, Hydar, Ferguson, Frederick, and Zhang, Shenygong. *An Engineering Method for the Construction and Analysis of Hypersonic Vehicle Configurations.,* 13th AIAA/CIRA International Space Planes and Hypersonic Systems and Technologies, Italy, May 16th – 20th, 2005, AIAA Paper 2005 – 3364.

[2] Apdin, Hydar. *An Engineering Method for the Design and Analysis of Waverider Derived Hypersonic Vehicles.,* M.S. Thesis, North Carolina A&T State University, 2004.

[3] Nonweiler, Terrence. *Re-entry Vehicle with High Lift Capabilities.,* U.K., 1959.

[4] Scott, Jeff, *Hypersonic Waveriders., 2000.*

[5] Nonweiler, T., "Aerodynamic Problems of Manned Space Vehicles," Journal of Royal Aeronautical Society, Vol. 67, Jan. 1963.

[6]Nonweiler, T., "Delta wings of Shapes Amendable to Exact Shock Wave Theory," Journal of Royal Aeronautical Society, Vol. 67, Jan. 1963.

[7]Bowcutt, Kevin G., Anderson, John D. Jr., and Capriotti, D.P., "Viscous Optimized Hypersonic Waveriders," AIAA paper 87-0272, 1987.

[8]Ferguson, F., "Expanding the Waverider Design Space Using Arbitrary Generating Flowfields", Ph.D. Dissertation, Department of Aerospace Engineering, University of Maryland, College Park, Maryland, 1993

[9]John D.Anderson "Fundamentals of Aerodynamics" Third Edition, 2001, McGRAW-HILL.

[10]Young, A.D., "Modern Developments in Fluid Dynamics', Vol. 1, High Speed Flow, Oxford University Press, 1953

[11]Bowcutt, Kevin G., "Optimization of Hypersonic Waveriders Derived from Cone Flows Including Viscous Effects", Ph.D. Dissertation, Department of Aerospace Engineering, University of Maryland, College Park, Maryland, 1986

[12]Hilerath, J., "Tables of Thermal Properties of Gases", National Bureau of Standards Circular 564, November 1955

[13]McLaughlin, Thomas A., "Viscous Optimized Hypersonic Waveriders for chemical Equilibrium Flow", M.S. Thesis, Department of Aerospace Engineering, University of Maryland, College Park, Maryland, 1990, UM-AERO-90-17.

[14]Anonymous, "U.S. Standard Atmosphere", 1976, U.S. Government Printing Office, Washington D.C., Oct. 1976.

[15]NASA Glenn Research Center, URL:http://www.grc.nasa.gov/WWW/K-12/airplane/atmosmet.html, Feb.15, 2005.

[16]William H. Heiser, David T. Pratt "Hypersonic Airbreathing Propulsion." AIAA Education Series. ISBN: 1-56347-035-7, Published by American Institute of Aeronautics and Astronautics. Inc 1994.

[17]Kuchemann, D. "The Aerodynamic Design of Aircraft", Pergamon Press, New York, 1978.